JACS
JOURNAL OF THE AMERICAN CHEMICAL SOCIETY
Article
pubs.acs.org/JACS

Bioinspired Artificial Single Ion Pump

Huacheng Zhang,[†,¶] Xu Hou,[‡,¶] Lu Zeng,[§] Fu Yang,[§] Lin Li,[§] Dadong Yan,[⊥] Ye Tian,*[,†] and Lei Jiang*[,†]

[†]Beijing National Laboratory for Molecular Sciences (BNLMS), Key Laboratory of Organic Solids, Institute of Chemistry, Chinese Academy of Sciences, Beijing 100190, P. R. China

[‡]National Center for Nanoscience and Technology, Beijing 100190, P. R. China

[§]College of Chemistry and [⊥]Department of Physics, Beijing Normal University, Beijing 100875, P. R. China

Supporting Information

ABSTRACT: Bioinspired artificial functional nanochannels for intelligent molecular and ionic transport control at the nanoscale have wide potential applications in nanofluidics, energy conversion, and biosensors. Although various smart passive ion transport properties of ion channels have been artificially realized, it is still hugely challenging to achieve high level intelligent ion transport features in biological ion pumps. Here we show a unique bioinspired single ion pump based on a cooperative pH response double-gate nanochannel, whose gates could be opened and closed alternately/simultaneously under symmetric/asymmetric pH environments. With the stimulation of the double-gate nanochannel by continuous switching of the symmetric/asymmetric pH stimuli, the bioinspired system systematically realized three key ionic transport features of biological ion pumps, including an alternating gates ion pumping process under symmetric pH stimuli, transformation of the ion pump into an ion channel under asymmetric pH stimuli, and a fail-safe ion pumping feature under both symmetric and asymmetric pH stimuli. The ion pumping processes could well be reproduced under a concentration gradient. With the advantages of the extraordinary ionic transport functions of biological ion pumps, the bioinspired ion pump should find widespread applicability in active transportation-controlling smart nanofluidic devices, efficient energy conversions, and seawater desalinization, and open the way to design and develop novel bioinspired intelligent artificial nanochannel materials.

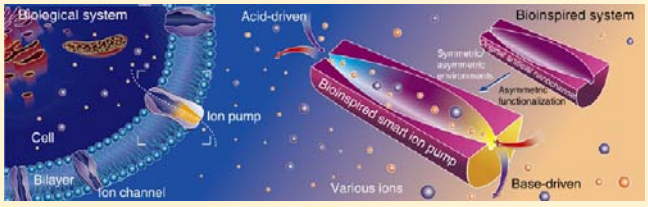

INTRODUCTION

Ion pumps and ion channels,[1−5] which exist in a cell membrane to intelligently control ions into and out of the membrane, are essential for various vital processes including maintaining cellular ion homeostasis,[3,6] signal transduction,[7] and energy conversion.[8] Unlike ion channels in which ionic and molecular transport is often simply governed by one single gate,[4] ion pumps generally refer to two cooperative response gates that are located separately at two ends of the pathway (Figure 1a (left)).[2,3] The two gates can open and close alternately or simultaneously, which makes ion pumps possess three unique ion transport features, including the alternating gates ion pump feature, the reversible transformation of ion pump into ion channel feature, and the fail-safe ion pump feature, compared with single-gate ion channels of simplex passive ionic transport properties (see Text S1 and Figure S1a−d in Supporting Information for detailed function differences between ion pumps and channels).[3] Recently, bioinspired nanochannels[9−11] have successfully reproduced various kinds of passive ionic transport properties of biological ion channels by integrating diverse chemical and physical stimuli like voltage,[12] pH,[13−15] light,[16,17] ion,[18,19] temperature,[20,21] pressure,[22] and ATP[23,24] with corresponding responsive molecules. The functional molecule immobilized on the certain shaped nanochannel could act as a stimulus-driven artificial gate that opens and closes in response to external stimulus alternation to functionally control ion transport through the bioinspired ion channels. However, as for the ion pumps, their three extraordinary ionic transport features are achieved on the basis of the two functional cooperative response gates controlling different highly intelligent ion pumping processes. So it is still a huge challenge to experimentally a build bioinspired artificial single ion pump.

In this work, we report a bioinspired smart single ion pump based on a unique cooperative pH response double-gate nanochannel (Figure 1a, right). Two separate acid- and base-driven gates immobilized on the small tip sides of a single cigar-shaped nanochannel could be alternately/simultaneously opened and closed under symmetric and asymmetric pH stimuli, which successfully mimics the cooperative response double gates of biological ion pumps. By continuously stimulating the two gates with the symmetric/asymmetric pH stimuli, the bioinspired double-gate nanochannel system systematically realized three essential ion transport features including alternating gates ion pump, reversible transformation of ion pump into ion channel, and fail-safe ion pump in nature (see Text S1 and Figure S1f−h in Supporting Information for systematical demonstration of the artificial single ion pump system). The ion pumping processes could well be reproduced

Received: April 16, 2013
Published: June 17, 2013

   dx.doi.org/10.1021/ja4037669 | J. Am. Chem. Soc. 2013, 135, 16102−16110

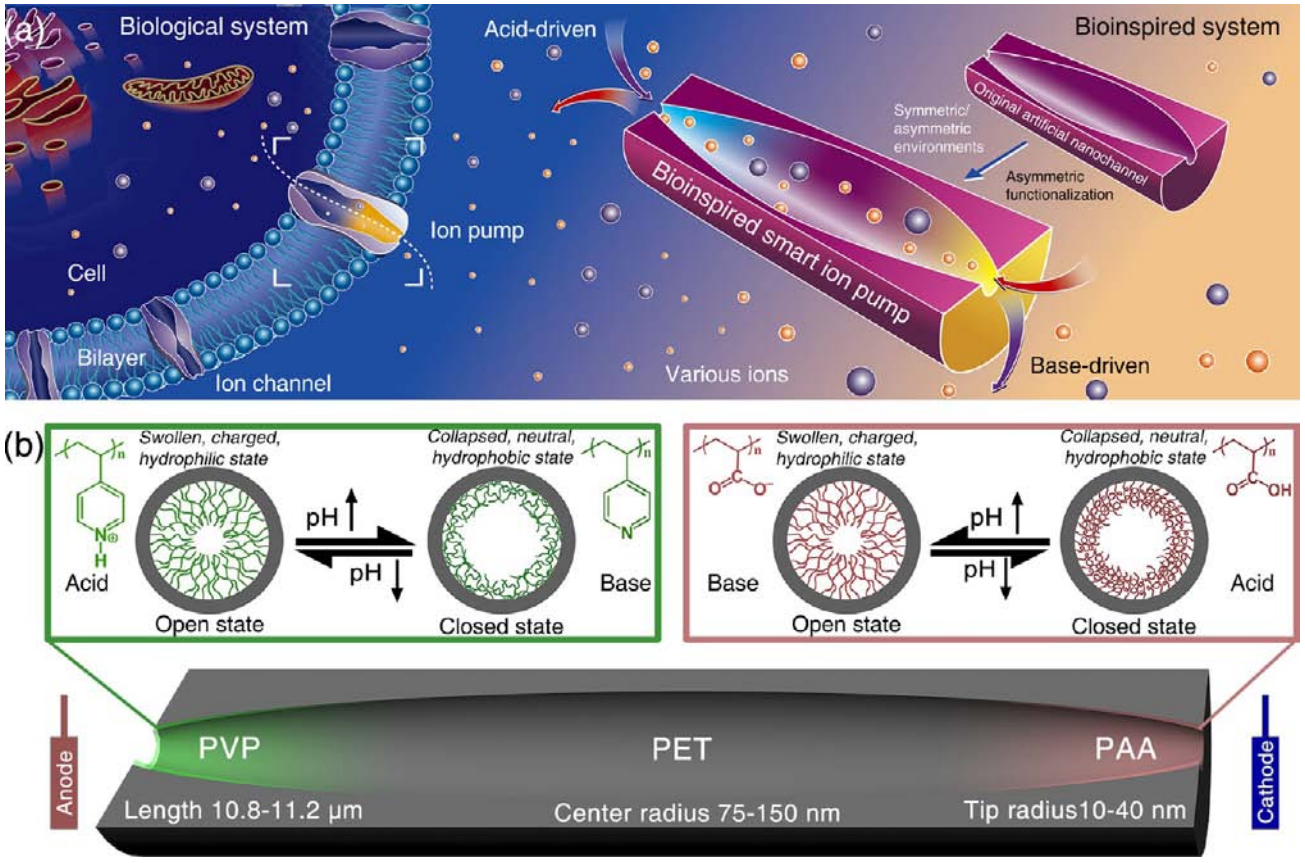

Figure 1. Bioinspired artificial functional single ion pump. (a) Drawing showing a biological system (left), in which the ion pump as a membrane-spanning pore has two separate gates located separately on both sides of the pathway (the blue and yellow parts of the ion pump represent the two separate gates, respectively), and our bioinspired smart single ion pump by integrating acid- and base-driven artificial gates into a single cigar-shaped nanochannel (right). (b) Schematic representation of cross section of the artificial cooperative pH response double-gate nanochannel that acid-driven PVP gate and base-driven PAA gate were respectively immobilized on the inner surface of the left and right tip sides of the nanochannel. During the pH changes within a certain range on the PVP side, PVP underwent pH-responsive conformation changes from the open state (acid condition) to the closed state (base condition) (left and up). At the same time, PAA underwent pH-responsive conformation transition between the closed state (acid condition) and the open state (base condition) (right and up).

under a concentration gradient. Such a system, as an example, demonstrates a development of artificial nanochannels from bioinspired ion channels to bioinspired ion pumps, and may lead to the new generation of intelligent nanochannel materials with diverse active ionic transportation features.

Ionic transport controls inside the biological ion pumps are mainly governed by their stimuli-driven changes of the shape and surface properties to alternately form open and closed gating states at end parts of the proteinacious passageways to finish ions exchange at the two sides of the cell membranes.[1,3,25] In the view of structure, here we selected the single cigar-shaped nanochannel as the platform to develop the bioinspired artificial single ion pump because, in contrast with other (cylinder,[26] cone,[14,18,20,27−29] hourglass,[30−32] and bullet[33−35]) shaped nanochannels,[36] it has two separate small tips on each side and a large center in the middle that satisfy all needs of building two separate gates and reserving space of ion storage in the ion pump system. Moreover, the surface properties of the two exposed tip sides of the cigar-shaped nanochannel could be directly and separately modulated by external pH stimuli to effectively control ion transport inside the nanochannel,[13] which lays the foundation for further building double cooperative pH response gates.

To realize all kinds of stimuli-gating ionic transport controls inside the nanochannels, functional molecules including small organic molecules,[16,28,30,37−39] polymers,[15,20,21,27,31,32] and biomolecules[12,14,18,19,23,24,40−43] have been used to functionalize nanochannels to build artificial functional gates on the bioinspired nanochannel by symmetric and asymmetric chemical modification methods.[36] However, compared with small organic molecules which could only change the surface charge distributions[28,30] of the nanochannels, functional polymers and biomolecules are able to change both sizes and chemical properties of the nanochannels[14,20,21,26,32] at the nanoscale by their ambient stimuli-driven conformational conversions to develop new stimuli-responsive nanochannel architectures. The stimulus-driven conformational conversions could well simulate protein channels where their functioning is determined by stimulus-triggered organization of the protein structure.[44,45] Moreover, polyelectrolytes have been used to realize more effective symmetric[26] and asymmetric[31,32] pH-gating ionic transports inside the nanochannels via their pH-responsive conformational transitions to change the size, surface charge, and wettability of the nanochannels.[44−47]

To effectively build cooperative response double gates onto the single nanochannel, two opposite pH-responsive polyelectrolytes, polyvinylpyridine (PVP) and poly(acrylic acid) (PAA), were separately grafted onto the left and right tip sides of the cigar-shaped nanochannel by a well-developed asymmetric modification method[36] (Figure 1b). PVP could

dx.doi.org/10.1021/ja4037669 | J. Am. Chem. Soc. 2013, 135, 16102−16110

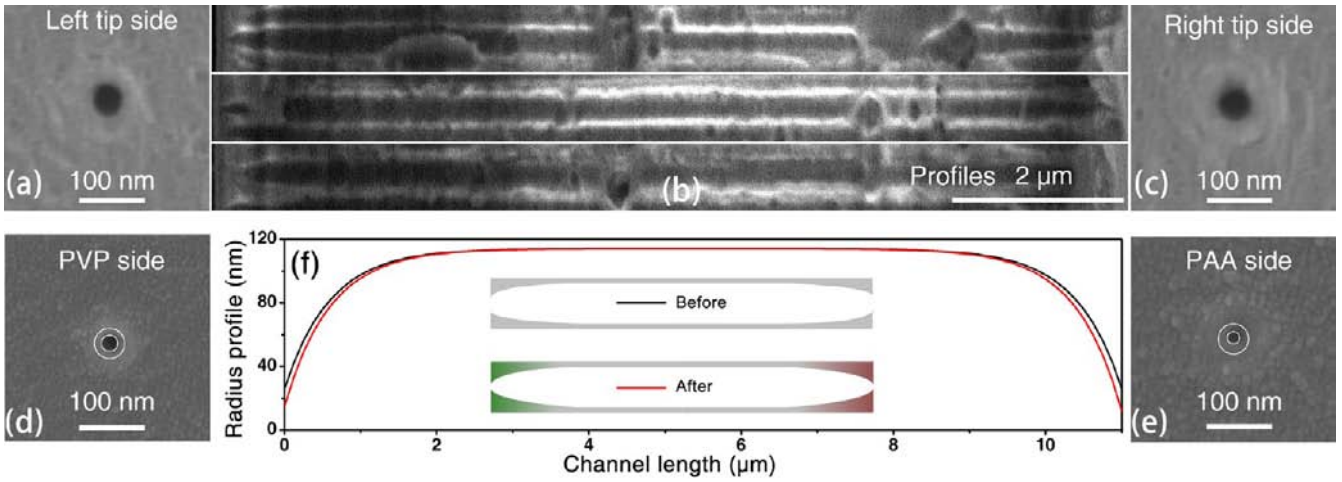

Figure 2. Dimension changes of the single cigar-shaped nanochannels before and after asymmetric PVP/PAA modification. (a–c) SEM images of the left tip side, cross sections, and the right tip side of the single nanochannel before modification. (d,e) SEM images of the PVP and PAA tip sides of the nanochannel after modification. The inset large and small white circles in the SEM images were used to respectively represent the sizes of the same tip side before and after modification. The region between the two white circles illustrates the thickness of the polymer gates. (f) Average radius profiles of the nanochannel before (black line, r_t = 26 nm, r_c = 114 nm, L = 11 μm) and after (red line, r_t = 14 nm (left side), r_t = 12 nm (right side), r_c = 114 nm, L = 11 μm) modification by Supporting Information eq S2 confirmed that polymer gates were mainly immobilized on the tip regions of the nanochannel. The inset schematic representations of cross sections of the nanochannel were used to illustrate surface properties and size changes at the two tip regions after modification.

undergo pH-responsive conformational changes from the swollen, positively charged, and hydrophilic state (open state) when the pH is below p*K*a of 5.2, to the collapsed, neutral, and hydrophobic state (closed state) when the pH is above p*K*a (left and up).[26] However, PAA underwent pH-responsive conformation of the collapsed, neutral, and hydrophobic state (closed state) when the pH is below the p*K*a of 4.7 and of the swollen, negatively charged, and hydrophilic state (open state) when the pH was above the p*K*a (right and up).[32] These opposite pH-responsive conformational conversions could well induce open/closed, closed/open, open/open, and closed/closed gating states of the PVP/PAA gates when both sides of the nanochannel are under acid/acid, base/base, acid/base, and base/acid environments, and thus demonstrated cooperative pH response functionality. By continuously stimulating the double-gate nanochannel by the above four symmetric/asymmetric pH stimuli to open and close PVP and PAA gates alternately/simultaneously, the bioinspired system could reproduce the three unique ionic transport features of biological ion pumps.

■ RESULTS AND DISCUSSION

The single cigar-shaped nanochannels embedded in polyethylene terephthalate (PET) membranes were prepared by surfactant controlling and ion track-etching technology.[36,48] The small opening of both sides of the channel was called "tip", while the large middle section was called "center" (Figure 1b, bottom). Scanning electron microscope (SEM) images illustrated symmetric small tip sides and cross sections of the cigar-shaped nanochannels (Figure 2a–c), The radii of tips and centers were studied and analyzed from multichannel membranes prepared under the same condition as single-channel membranes by SEM, due to the difficulty of huge amounts of locating both tip and center of the single nanochannel membranes in SEM for the efficient shapes analysis. The radii of tip and center follow Gaussian distribution (see Text S2 and Figure S2b,c in Supporting Information). Tip radius (r_t) ranged from ~10 nm to ~40 nm, and the calculated average value was 26 ± 5 nm. Center radius (r_c) ranged from ~75 nm to ~150 nm, and the calculated mean value was 114 ± 16 nm. Thickness of the PET membrane after etching was from ~10.8 μm to ~11.2 μm, and length of the original nanochannel (L) with relevant standard deviations was 11.0 ± 0.1 μm. Moreover, to further prove the shape of the nanochannel is the symmetric cigar shape, the radius profiles of the single nanochannels, in which the scale of radius is along the horizontal axis (Figure S2a in Supporting Information), were experimentally obtained in Figure S2e (scatters, in Supporting Information), and a half radius profile of the nanochannel could be well fitted by an exponential function shaped as a half cigar (equation (eq) S1 and Figure S2d in Supporting Information). So a whole profile of the cigar-like nanochannel could be described by Supporting Information eq S2 due to its symmetric shape, and moreover the fitting curve shows a mean trend of the experimental profiles of the nanochannels (see Figure S2e (red line) in Supporting Information). Therefore, the consistence of experimental statistical results and theoretical calculating data of the single nanochannels greatly confirmed their symmetric cigar shape.

As shown in Figure 2d, the SEM images of the left tip side of the nanochannel after PVP modification illustrated that the diameter of the tip side was reduced after grafting PVP, and the average radius of the tip sides after PVP modification was about 14 ± 3 nm. The inset large and small white circles in the SEM image were used to separately represent the sizes of the tip side before and after modification, where the region between the two white circles illustrated the thickness of the PVP gate, which was equal to the decreased radius of the tip side of the nanochannel, and the average thickness of the PVP gate was about 12 nm. At the same time, the radius of the right tip sides of the nanochannels also correspondingly decreased to about 12 ± 3 nm after PAA modification (Figure 2e), and the average thickness of the PAA gate was about 14 nm. Thus, the thickness of the PAA gate would be slightly higher than that of the PVP

dx.doi.org/10.1021/ja4037669 | J. Am. Chem. Soc. 2013, 135, 16102–16110

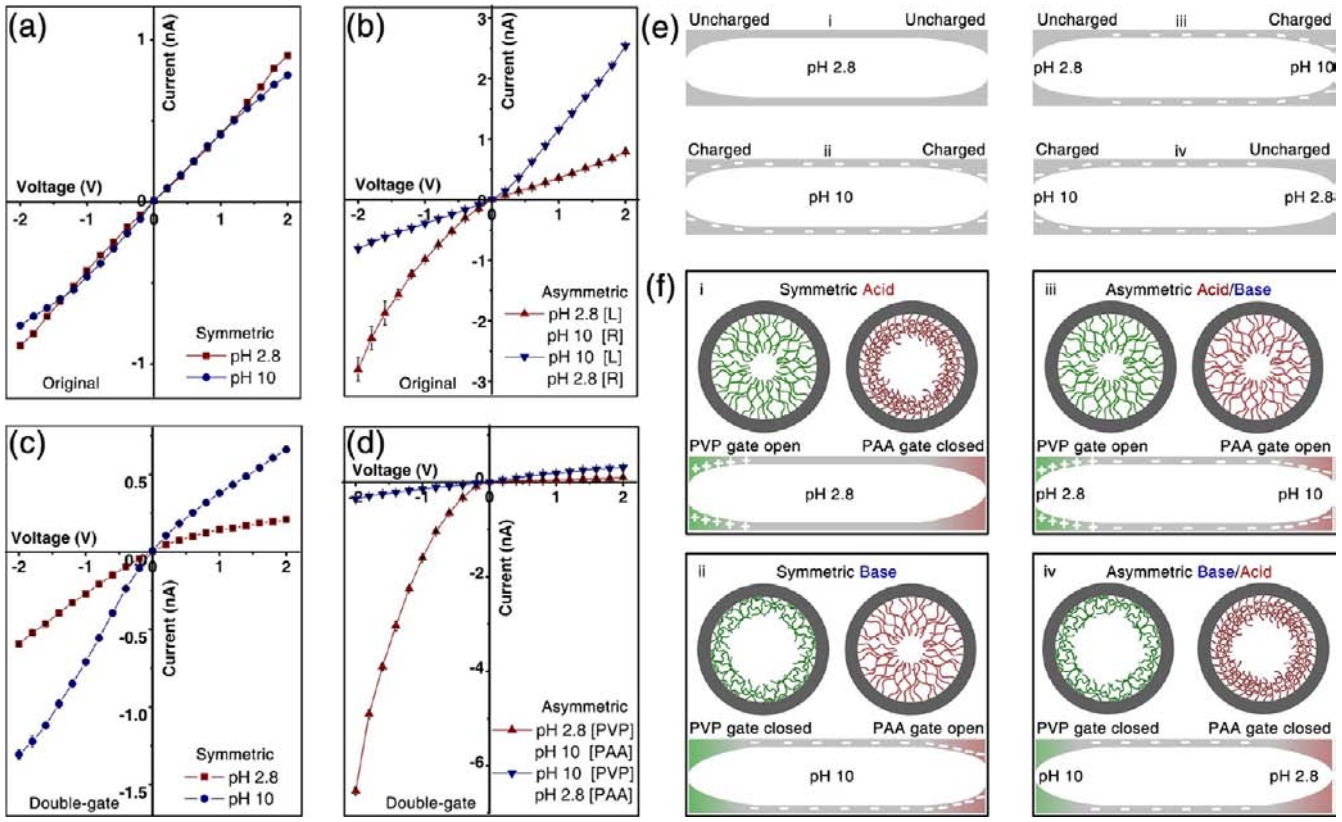

Figure 3. Cooperative pH response double gates. (a–d) *I–V* curves of the original (a,b) and double-gate (c,d) nanochannel under symmetric pH 2.8 (wine squares) and 10 (blue circles), and asymmetric pH 2.8/10 (wine up triangle) and 10/2.8 (blue down triangle) conditions illustrated functional ion transport control inside the nanochannel by the double opposite pH-responsive gates. (e,f) Schematic representations of the nanochannel surface properties change before (e) and after (f) modification under the symmetric and asymmetric pH stimuli (i, pH 2.8/2.8; ii, pH 10/10; iii, pH 2.8/10; iv, pH 10/2.8). Compared to sole surface charge variation of the original nanochannel resulting from protonation and deprotonation of the surface carboxyl group, surface properties of the double-gate nanochannel including surface charge, radius, and wettability were effectively modulated by alternate and simultaneous opening and closure of the two cooperative response polymer gates under different pH stimuli. Positive and negative surface charges were denoted by the symbols of "+" and "−", respectively.

gate in the single nanochannel under similar modification conditions.

To further confirm that the asymmetric PVP/PAA modification mainly occurred at the tip region of the nanochannel, resistances of the single nanochannels before and after modification were examined by measuring the ionic current across the nanochannel in 1 M KCl solution at 23 °C (Figure S3a in Supporting Information). Seven single nanochannels fabricated under the same condition were measured here to get the resistance changes of the nanochannel before and after PVP/PAA modification. Observed resistances of the seven nanochannels after modification (samples 1–7) were 2.0, 2.4, 2.7, 1.7, 2.1, 1.6, and 1.8 times higher than the resistances of the nanochannels before modification (see Table S1 in Supporting Information). Averaged results demonstrated that the resistance of a nanochannel could be increased by about 2 times after modification. The asymmetric PVP/PAA modification in our work could be theoretically supposed to two cases: the uniform thickness of grafted polymers that polymer brushes were homogenously grafted on the whole inner surface of the nanochannel, and the un-uniform thickness of the polymer layer which quickly decreased at the tip area of the nanochannel due to exponential growth of size of the nanochannel at this region. In the previous case, the resistance of the nanochannel after modification should theoretically increase by about 4 times (by Supporting Information eq S3) compared to original nanochannel, which was not consistent with our experimental result of ∼2 times. However, in the latter case, resistance of the modified nanochannel was twice higher than that of the original nanochannel, which was in accordance with the experimental result. So PVP and PAA brushes were mainly immobilized on the tip regions of the nanochannel after modification. As shown in Figure 2f, the average radius profiles before (black line) and after (red line) modification from Supporting Information eq S2 well illustrated that the size of the nanochannel was mainly reduced at both tip regions. Schematic representations of cross sections of the nanochannel before and after modification were used to illustrate surface properties and sizes changes at the two tip regions (Figure 2f, insets). Additional XPS measurements before and after modification also confirmed the successful bonding of the two separate polymer gates on the both sides of the nanochannel (see Figure S3f,g and Tables S2 and S3 in Supporting Information).

To inspect and verify the cooperative pH response functionalities of the two polymer gates, current–voltage (*I–V*) properties of the nanochannel before and after modification have been examined in 0.1 M KCl solution at 23 °C integrating with symmetric pH 2.8/2.8 and pH 10/10 stimuli, and asymmetric pH 2.8/10 and pH 10/2.8 stimuli. Figure 3 shows observed *I–V* curves (Figure 3a–d) and corresponding surface properties (Figure 3e,f) of the nanochannel (sample 1)

dx.doi.org/10.1021/ja4037669 | J. Am. Chem. Soc. 2013, 135, 16102–16110

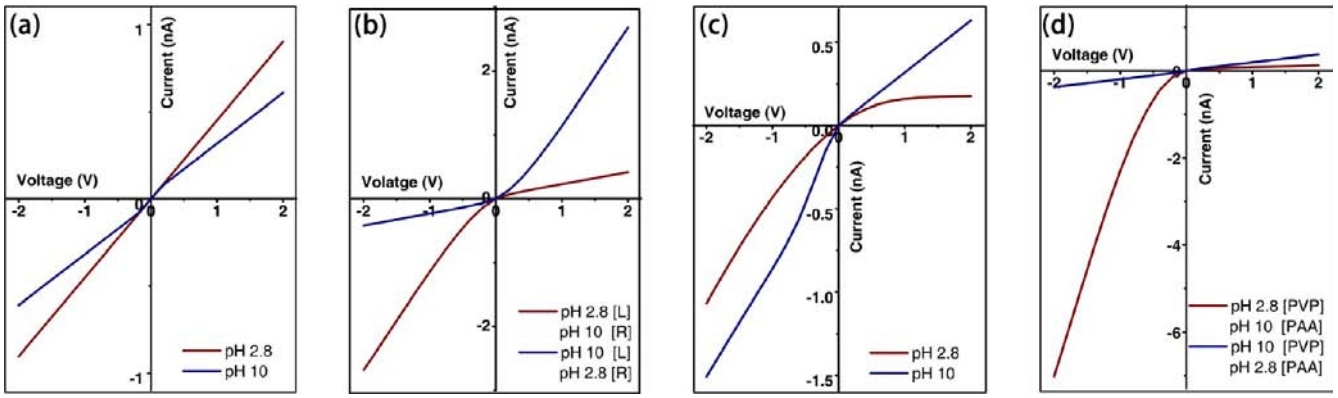

Figure 4. Theoretical $I-V$ curves of the original (a,b) and double-gate (c,d) nanochannel (sample 1) under symmetric pH 2.8 (wine) and 10 (blue), and asymmetric pH 2.8/10 (wine) and 10/2.8 (blue) conditions from the PNP model show good agreement with the experimental $I-V$ curves in Figure 3a–d (see Text S4 and Figures S4 to S6 in Supporting Information for detailed theoretical discussions).

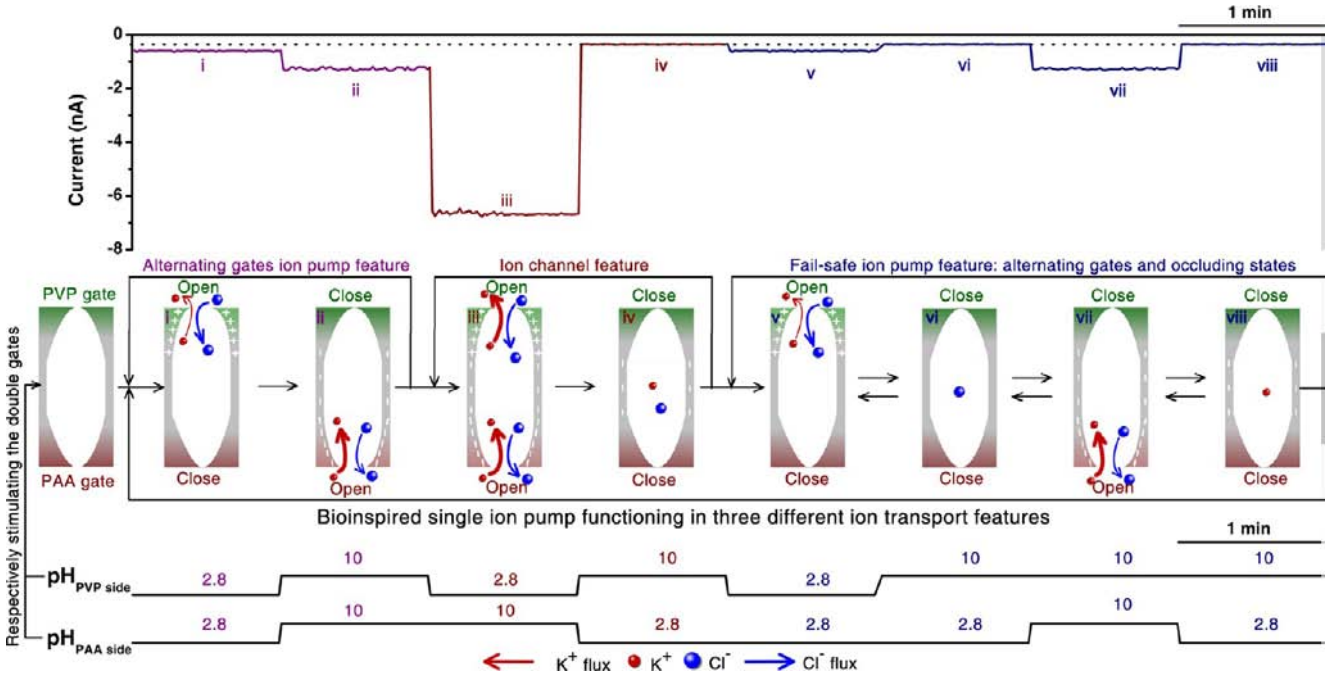

Figure 5. Bioinspired artificial functional single ion pump functions in three different ion transport features. Ion current states (up) and corresponding schematic representations of ion transport processes (middle) of the three ion transport features resulting from respectively stimulating the double gates of the nanochannel by manually continuous pH stimuli switching (down) at −2 V. Alternating-gates ion pump under symmetric pH stimuli (left, violet), in which PVP and PAA gates opened and closed alternately to enable exchange of K^+ for Cl^- ions across the nanochannel (i and ii). Ion channel-like function under asymmetric pH stimuli (center, wine) that both PVP and PAA gates were simultaneously opened/closed to directly transport/block ions from one side to the other side (iii and iv). Fail-safe ion pump function (right, blue) consists of alternating gates (v and vii) and occluding states (vi and viii) under both symmetric and asymmetric pH stimuli.

before and after modification. Before modification, the nanochannel exhibited symmetric linear and S-type $I-V$ curves under symmetric pH 2.8 and 10 conditions (Figure 3a). During the nanochannel preparing process, negatively charged carboxyl groups were created on the channel surface when the pH was above the PET pKa of 3.8. Thus, it is apparent that the change of ionic transport symmetric properties between linear and S type is caused by the symmetric inner surface charge of the nanochannel (Figure 3e,ii). The degree of ionic rectification, was defined as the ratio$_{\mp}$ of absolute values of ionic currents recorded at a given negative voltage (−2 V, anode facing the PAA side of the nanochannel) and at the same absolute value of a positive voltage (+2 V, anode facing the PVP side of the nanochannel), ratio = $|I_{-2\ V}|/|I_{+2\ V}|$. However, the $I-V$ properties become asymmetric with the approximately reciprocal relation of the ion current rectification degrees (ratios of 3.53 ± 0.06 and 0.32 ± 0.03) under the two opposite asymmetric pH 2.8/10 and 10/2.8 conditions. These asymmetric phenomena were attributed to the uneven surface charge distributions[49] that could rectify ion current across the nanochannel (Figure 3e,iii and iv).

After modification, however, the rectifications were observed as asymmetric $I-V$ curves appeared under symmetric pH conditions, and there was a significant increase in the transmembrane ion current when the pH changed from 2.8 to 10 (Figure 2c). Because the PVP gate is acid-driven and the PAA gate is base-driven, only one of the polymer gates could be opened at a time under symmetric acid and base conditions.

dx.doi.org/10.1021/ja4037669 | J. Am. Chem. Soc. 2013, 135, 16102–16110

Under the symmetric pH 2.8 condition, the PVP gate opened to a swollen, positively charged, and hydrophilic state, but the PAA gate closed to a collapsed, hydrophobic, and uncharged state (Figure 3f,i). While the polymer gates changed into their opposite states under symmetric pH 10 condition (Figure 3f, ii). As a result, the asymmetric ion transport properties of the nanochannel under symmetric pH conditions were attributed to the uneven surface charge distribution and wettability induced by the alternative opening of two polymer gates. The ionic currents of the nanochannel at symmetric pH 10 are higher than that at pH 2.8 because the unmodified center of the nanochannel was negatively charged under the pH 10 condition which increased the conductance of the nanochannel. Besides, a remarkable change between the rectified (ratio of 65.27 ± 0.05) and the near linear (ratio of 1.14 ± 0.01) ion transport properties of the double-gate nanochannel was observed under asymmetric pH 2.8/10 and 10/2.8 conditions, respectively (Figure 3d). The two gates were simultaneously opened and closed by the asymmetric pH conditions, leading to extreme asymmetric surface charge distribution and nearly symmetric surface properties under these two opposite asymmetric pH conditions (Figure 3f,iii and iv). Therefore, different from the sole pH-responsive surface charge controlling ion transport of the original nanochannel (Figure 3e), ion transport of the double-gate nanochannel was intelligently controlled by the double cooperative pH response gates that open and close alternately and simultaneously in response to external pH change, and further manipulate the surface properties of the nanochannel including charge distribution, size, and wettability (Figure 3f).

The aforementioned experimental results can be further theoretically proved by a continuous Poisson−Nernst−Plank (PNP) theory[50−53] on the basis of surface charge distributions of the nanochannel shown in Figure 3e,f. To get the theoretical results more directly and avoid complex calculation processes, here we simplify the double-gate nanochannel to a simple system where charges of polymer gates were strictly confined to the nanochannel walls, and influences of the channel size and wettability variations induced by polymer gates on the ionic transport properties were also neglected. As shown in Figure 4, the theoretical $I-V$ curves of the nanochannel (Sample 1) before and after modification from PNP model show excellent agreement with the experimental observations (Figure 3a−d) (see Text S4 and Figures S4 to S6 in Supporting Information for detailed theoretical discussions).

On the basis of the cooperative pH response double gates, unidirectional ion pump-like ion transport controls inside the double-gate nanochannel were intuitionally demonstrated by continuously regulating ion transport states of the nanochannel at −2 V (Figure 5, also see Text S5 and Figure S7 in Supporting Information for unidirectional ion transport). It is worth mentioning that the applied voltage acts as the external energy source to drive ions into and out of the nanochannel in the system. Moreover, gating abilities of the two polymer gates were well controlled by the thickness of grafted polymer layers to make the artificial ion pump system more close to the biological ion pumps when two gates could completely block ionic transport on their closed states. However, in the bioinspired system, two artificial polymer gates are designed to keep low ion conductivity under the closed state to ensure all ion current states could be detected due to the limited characterization methods of ion pumps (see Text S6 and Figure S8 in Supporting Information).

We first reproduced ionic transport control as a biological alternating gates ion pump by continuously and alternately opening the two polymer gates under symmetric pH stimuli (Figure 5 (left, violet)). The nanochannel was activated by symmetric pH 2.8/2.8 conditions, and the PVP gate was first opened, allowing Cl^- ions to move in and K^+ ions to move out of the nanochannel under the electric force driving, while the PAA gate was closed and blocked the ion transport on its side, which induced a low ion current state (about −0.59 ± 0.01 nA, Figure 5,i). Then by shifting the exterior pH to symmertic10/10, the PVP gate was closed and the PAA gate was opened. Therefore, ion transport was stopped on the PVP side but started on PAA side, and resulted in a low ion current under this state (about −1.55 ± 0.03 nA, Figure 5,ii). Hence, by combining these two ion transport states, an entire ion transport process of ion pumping is accomplished, which perfectly mimics the biological ion pumps with two alternating gates,[54] i.e., Na^+/Ca^{2+} ion pumps (Figure S1b,f in Supporting Information).[55]

Besides, the nanochannel could also be transformed into an ion channel by the simultaneous opening/closing of the two polymer gates under asymmetric pH stimuli (Figure 5 (center, wine)). The transmembrane ion current was very high under asymmetric pH 2.8/10 conditions because both PVP and PAA gates were opened simultaneously, and ions could quickly flow from one side to the other side (about −6.70 ± 0.17 nA, Figure 5,iii). In contrast, ion current was rather low when both gates were closed, and ions were occluded inside the nanochannel under asymmetric pH 10/2.8 condition (about −0.31 ± 0.02 nA, Figure 5,iv). The continuous switching of these two opposite asymmetric pH conditions caused the nanochannel to function like the ion channel in which the ion currents alternated between high and low states by simultaneously opening/closing the two polymer gates (Figure 5,iii and iv; and also see Figure S1c,g in Supporting Information). External pH stimuli alternating between symmetric and asymmetric leads to reversible switching of the nanochannel functions between ion pump and ion channel, which is also a common phenomenon in ion pumps.[56]

Furthermore, to avoid functioning like ion channels by opening/closing gates simultaneously, the biological ion pumps have evolved a fail-safe ion transport mechanism in which both gates first close, occluding ions inside the protein even before the second gate is able to open to release them, such as Na^+/K^+ or Ca^{2+} ATPase ion pumps.[25,57] Like biological ion pumps, the fail-safe ion transport processes were reproduced by integrating symmetric pH stimuli with asymmetric pH 10/2.8 conditions in this artificial ion pump (Figure 5 (right, blue); and Figure S1h in Supporting Information). First the nanochannel was activated with a symmetric acid condition, the PVP gate was opened to allow Cl^- ions to move into and K^+ ions to move out of the nanochannel, and low ion current was characterized (Figure 5,v). Then the PVP gate was closed by changing the pH of its side to 10, ions (most of them were Cl^-) were timely occluded inside the nanochannel, and little ion current was measured (Figure 5,vi). Subsequently, to release Cl^- ions on the other side and to collect K^+ ions into the nanochannel, the PAA gate was opened by stimulating it with pH 10, and the ion current slightly increased (Figure 5,vii). Following closure of the PAA gate by reducing the pH of its side to 2.8, ions (most of them were K^+) were occluded in the nanochannel again, and ion current ceased (Figure 5,viii). As a result, by simply and orderly changing external pH stimuli, the artificial system could

systematically reproduce ionic transport processes of the three essential ion transport features in biological ion pumps.

To further illustrate differences in the three features more comprehensively, the ion current of a whole ion transport process was averaged to indicate the ion transport capability under each ionic transport feature. Different from direct movement of ions through the nanochannel under the open state in ion channel function (iii), ions transporting from one side to the other side in ion pump and fail-safe ion pump functions must respectively undergo two (i and ii) and four (v to viii) ion transport states (Figure 5). Therefore, ion transport capability is the lowest in fail-safe ion pump function of −0.65 ± 0.02 nA and highest in ion channel function of −6.70 ± 0.17 nA, which is consistent with biological systems.[3] To further confirm the reversibility and stability of the bioinspired system, pH stimuli were orderly switched in three cycles, and resulting stable ion transport capabilities of the three features were shown in Figure 6b–d. Additional samples also proved that the artificial ion pump system has good reproducibility (see Text S7 and Figures S9 and S10 in Supporting Information).

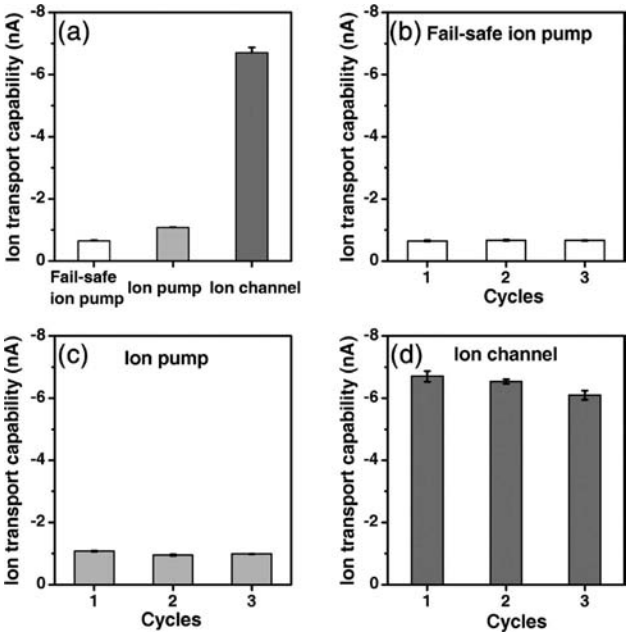

Figure 6. (a) Ion transport capabilities of the artificial ion pump functioning in the three different functions. (b–d) Stability of the artificial system was characterized by the ion transport capability of the three ion transport features.

Considering the biological ion pumps work under transmembrane asymmetric ion concentration environments to pump ions from the low concentration side to the high concentration side, we further investigated the functionalities of this bioinspired artificial single ion pump under a concentration gradient of 0.01 M/0.1 M, the PVP side of 0.01 M KCl and PAA side of 0.1 M KCl, and a reproduced double-gate nanochannel (sample 3) was used in this experiment (see Text S8 and Figure S11 in Supporting Information). When the sample 3 was stimulated by the continuous switching of pH stimuli in a symmetric concentration environment of 0.1 M/0.1 M, ion current states of the three different ion transport features were also observed (Figure 7, black line). However, significant enhancement and decrease of the ion current sates were separately obtained in ion pump and ion channel

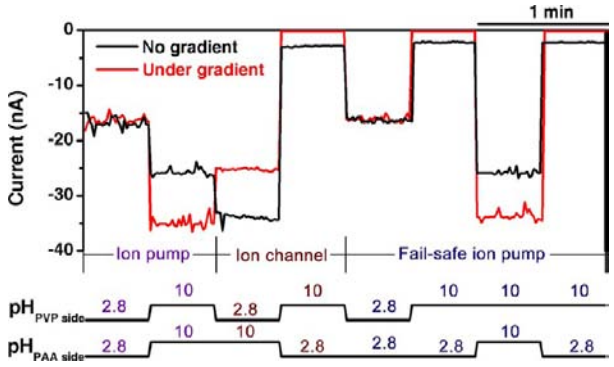

Figure 7. The artificial single ion pump works well under concentration gradient. Ion current states (up) of the artificial ion pump in the three different ion transport features under (red) and without (black) concentration gradient at −2 V and corresponding pH stimuli (down).

functions under the concentration gradient, which reproduced the ion transport phenomenon of biological systems where the ion pump could work under both symmetric and asymmetric concentration environments, but ion channel are influenced by external concentration gradient (Figure 7, red line).

Ion transport capabilities of the artificial ion pump system increased in ion pump function but reduced in ion channel function under concentration gradient, which also confirmed that the bioinspired ion pump system could operate well both with and without a concentration gradient in the ion pump function (Figure 8). The system possessed a similar trend of

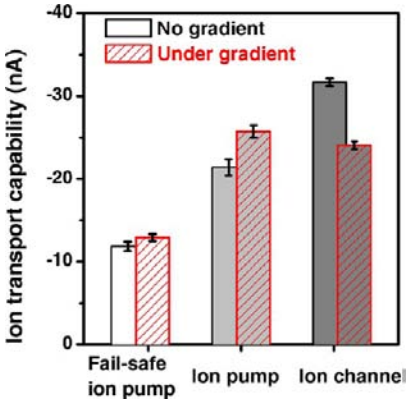

Figure 8. Ion transport capabilities of the three different ion transport features under and without concentration gradient.

ion transport capability change in the ion pump and fail-safe ion pump functions. The ion pumping processes could also be reproduced under a concentration gradient.

CONCLUSIONS

In summary, we have experimentally and theoretically demonstrated a bioinspired single ion pump system based on an artificial cooperative pH response double-gate nanochannel. The bioinspired system systematically realized three essential ion transport features including an alternating gates ion pump feature, reversible transformation of ion pump into an ion channel feature, and fail-safe ion pump feature existing in the biological ion pumps through manually stimulating the double gates by symmetric and asymmetric pH stimuli. Moreover, the system could also reproduce ion pump features well under a

dx.doi.org/10.1021/ja4037669 | J. Am. Chem. Soc. 2013, 135, 16102–16110

concentration gradient. This work as an example demonstrated the feasibility of the design strategy of building bioinspired single ion pumps working under various stimuli, and may also open the way to develop diverse functional ion pumps by artificial single nanochannels to satisfy the real application in nanofluidic devices, biosensors, and seawater desalination devices. As biological ion pumps are natural energy conversion devices, the bioinspired ion pumps may have potential for constructing the artificial high efficient energy conversion devices[58] that covert energy from assorted sources such as light, temperature, and mechanical forces, to potential energy stored in an electrochemical gradient.

EXPERIMENTAL SECTION

Nanochannels Preparation. The single cigar-shaped nanochannels were produced in PET membranes (Hostaphan RN12 Hoechst, 12 μm thick, with single or multi-ion tracks in the center) by integratively using both a surfactant-controlled etching method and an ion track etching technique.[48] To produce the cigar-shaped nanochannels, the irradiated membrane was etched from both sides with etching solution (6 M NaOH + 0.025% sodium dodecyl diphenyloxide disulfonate) at 60 °C. For observation of the etching process, the voltage (1 V) used to monitor the etching process was applied in such a way that the transmembrane ion current can be observed as soon as the nanochannel opened. Since both sides of the membrane were subjected to the surfactant-controlled etching, the effects of surfactant-controlled etching taking place simultaneously on each track end, which led to the etching rates of each end, were slower than the center. After about 6 min etching, both sides of the membrane were added to a 1 M KCl + 1 M HCOOH solution that was able to neutralize the etchant, thus slowing down and finally stopping the etching process. The obtained cigar-shaped nanochannels had two small tip sides and a large center. The diameters and profiles of the nanochannels were observed from the multichannel membranes fabricated in the parallel etching experiments by SEM.

Plasma-Induced Graft Polymerization. The PET membrane was soaked in water overnight after the etching experiment. There are two steps for our asymmetric chemical modification approach. In the first step, one side of the nanochannel was modified with PVP. VP was placed in a monomer delivery system (Suzhou Omega Machinery Electronic Technology Co., Ltd., DJ-02). The vacuum before switching on the glow discharge was 8 Pa, and the working temperature was maintained at 30 °C, because of the high volatility of VP. In our experiment setup, the loop of pumping and releasing argon gas in the reaction chamber (Suzhou Omega Machinery Electronic Technology Co., Ltd., DT-02) ran three times. Then, the reaction chamber was maintained at a power of 40 W to glow discharge. At the same time, the argon atmosphere was kept at about 50−60 Pa, and this process would last for 15 min. After the glow extinguished, VP monomers were transported to the reaction chamber, which continues for about 15 min with a vacuum degree of 20−40 Pa for the grafting reaction. After that, the chamber was connected with air. In the second step, the other side of the nanochannel was modified with PAA. Distilled AAc was injected into the plasma-induced grafting reactor (Suzhou Omega Machinery Electronic Technology Co., Ltd., DJ-02). The vacuum before switching on the glow discharge was 8 Pa and the working temperature was 30 °C. The argon atmosphere was kept about 50−60 Pa at 40 W to glow discharge and this process would last for 15 min. After the glow extinguished, the grafting reactor would lead to grafting AAc monomers, maintaining the vacuum degree of 50−70 Pa. It would last about 15 min for the grafting reaction. After that, the chamber was connected to air. The plasma treatment was finished. At present, the experimental results of pH-responsive ion transport properties of the nanochannel system as the indirect evidence favor the asymmetric chemical modification.

Current Measurement. The ion transport properties of the bioinspired system were studied by measuring ion current through the single nanochannels before and after plasma treatment. The ionic current measurements were carried out with a Keithley 6487 picoammeter (Keithley Instruments, Cleveland, OH) and Ag/AgCl electrodes in a custom-designed electrolyte cell, and the single-channel membrane was mounted between the two halves of the cell. Ag/AgCl electrodes were used to apply a transmembrane potential across the membrane. The anode faced the left (PVP gate) side of the nanochannel (Figure 1b).The main transmembrane potential used in this work had been evaluated beforehand, and a scanning voltage varied from −2 V to +2 V with a 40 s period was selected. The pH of the electrolyte was adjusted by 1 M HCl and KOH solutions, and the influence of addition substance quality can be ignored. Symmetric/asymmetric pH stimuli were built by adjusting pH values of solutions in the two halves of the cell. Symmetric pH stimuli, both sides of the nanochannel under same pH conditions; asymmetric pH stimuli, both sides under different pH conditions. It should be clear that all the pH values and ionic currents in this work are measured at 23 °C. All measurements were carried out in a custom-designed temperature control system. In this work, each test was repeated at least three times to obtain the average current value at different voltages on the same nanochannel.

ASSOCIATED CONTENT

Supporting Information

Differences of structure and functions between biological ion pumps and ion channels, more SEM images of the nanochannel before and after modification, equations to describe radius profiles and resistances of the nanochannels, experimental and theoretical radius profiles, XPS analysis, $I-V$ properties of the single nanochannel before and after modification in 1 M KCl, quantitative description of surface charge distributions, details of PNP model, theoretical $I-V$ curves, gating abilities of polymer gates and resulting ion transport capabilities of three ion transport features of the artificial ion pump under different gating abilities of the double gates, experimental $I-V$ curves and ion transport capabilities of reproduced three samples 1−3, and experimental $I-V$ curves under concentration gradient. This material is available free of charge via the Internet at http://pubs.acs.org.

AUTHOR INFORMATION

Corresponding Author

jianglei@iccas.ac.cn; tianyely@iccas.ac.cn

Author Contributions

[¶]H.Z. and X.H. contributed equally in this work.

Notes

The authors declare no competing financial interest.

ACKNOWLEDGMENTS

This research is supported by the National Research Fund for Fundamental Key Projects (2011CB935700, 2013CB932802, 2012CB933800, 2009CB930404, 2010CB934700, 2012CB933200), National Natural Science Foundation (21201170, 20920102036, 21121001, 91127025, 21171171, 11290163, 21071148) and the Key Research Program of the Chinese Academy of Sciences (KJZD-EW-M01). The Chinese Academy of Sciences is gratefully acknowledged. The authors thank K. Li (Institute of Chemistry, Chinese Academy of Sciences) and Z. Yang (College of Chemistry, Beijing Normal University) for help in experiments, and Prof. D. Qiu (Institute of Chemistry, Chinese Academy of Sciences) for beneficial discussions. We also thank the members of the Materials Research Department at the GSI Helmholtz Centre (Darmstadt, Germany) for preparation and irradiation of the polymer foils.

REFERENCES

(1) Gadsby, D. C. *Nature* **2004**, *427*, 795.
(2) Gouaux, E.; MacKinnon, R. *Science* **2005**, *310*, 1461.
(3) Gadsby, D. C. *Nat. Rev. Mol. Cell Biol.* **2009**, *10*, 344.
(4) Hille, B. *Ion Channels of Excitable Membranes*, 3rd ed.; Sinauer Associates: Sunderland, Massachusetts, 2001.
(5) Gadsby, D. C.; Kimura, J.; Noma, A. *Nature* **1985**, *315*, 63.
(6) Reyes, N.; Gadsby, D. C. *Nature* **2006**, *443*, 470.
(7) Catterall, W. *Science* **1988**, *242*, 50.
(8) Xu, J.; Lavan, D. A. *Nat. Nanotechnol.* **2008**, *3*, 666.
(9) Hou, X.; Guo, W.; Jiang, L. *Chem. Soc. Rev.* **2011**, *40*, 2385.
(10) Siwy, Z. S.; Howorka, S. *Chem. Soc. Rev.* **2010**, *39*, 1115.
(11) Hou, X. *Bio-inspired Asymmetric Design and Building of Biomimetic Smart Single Nanochannels*; Springer: Heidelburg, Germany, 2013.
(12) Harrell, C. C.; Kohli, P.; Siwy, Z.; Martin, C. R. *J. Am. Chem. Soc.* **2004**, *126*, 15646.
(13) Ali, M.; Ramirez, P.; Nguyen, H. Q.; Nasir, S.; Cervera, J.; Mafe, S.; Ensinger, W. *ACS Nano* **2012**, *6*, 3631.
(14) Xia, F.; Guo, W.; Mao, Y. D.; Hou, X.; Xue, J. M.; Xia, H. W.; Wang, L.; Song, Y. L.; Ji, H.; Ouyang, Q.; Wang, Y. G.; Jiang, L. *J. Am. Chem. Soc.* **2008**, *130*, 8345.
(15) Yameen, B.; Ali, M.; Neumann, R.; Ensinger, W.; Knoll, W.; Azzaroni, O. *J. Am. Chem. Soc.* **2009**, *131*, 2070.
(16) Wang, G.; Bohaty, A. K.; Zharov, I.; White, H. S. *J. Am. Chem. Soc.* **2006**, *128*, 13553.
(17) Brunsen, A.; Cui, J.; Ceolin, M.; Campo, A. d.; Soler-Illia, G. J. A. A.; Azzaroni, O. *Chem. Commun.* **2012**, *48*, 1422.
(18) Hou, X.; Guo, W.; Xia, F.; Nie, F. Q.; Dong, H.; Tian, Y.; Wen, L. P.; Wang, L.; Cao, L. X.; Yang, Y.; Xue, J. M.; Song, Y. L.; Wang, Y. G.; Liu, D. S.; Jiang, L. *J. Am. Chem. Soc.* **2009**, *131*, 7800.
(19) Tian, Y.; Hou, X.; Wen, L.; Guo, W.; Song, Y.; Sun, H.; Wang, Y.; Jiang, L.; Zhu, D. *Chem. Commun.* **2010**, *46*, 1682.
(20) Yameen, B.; Ali, M.; Neumann, R.; Ensinger, W.; Knoll, W.; Azzaroni, O. *Small* **2009**, *5*, 1287.
(21) Guo, W.; Xia, H. W.; Xia, F.; Hou, X.; Cao, L. X.; Wang, L.; Xue, J. M.; Zhang, G. Z.; Song, Y. L.; Zhu, D. B.; Wang, Y. G.; Jiang, L. *ChemPhysChem* **2010**, *11*, 859.
(22) Lan, W. J.; Holden, D. A.; White, H. S. *J. Am. Chem. Soc.* **2011**, *133*, 13300.
(23) Jiang, Y.; Liu, N.; Guo, W.; Xia, F.; Jiang, L. *J. Am. Chem. Soc.* **2012**, *134*, 15395.
(24) Liu, N.; Jiang, Y.; Zhou, Y.; Xia, F.; Guo, W.; Jiang, L. *Angew. Chem., Int. Ed.* **2013**, *52*, 2007.
(25) Morth, J. P.; Pedersen, B. P.; Toustrup-Jensen, M. S.; Sorensen, T. L. M.; Petersen, J.; Andersen, J. P.; Vilsen, B.; Nissen, P. *Nature* **2007**, *450*, 1043.
(26) Yameen, B.; Ali, M.; Neumann, R.; Ensinger, W.; Knoll, W.; Azzaroni, O. *Nano Lett.* **2009**, *9*, 2788.
(27) Yameen, B.; Ali, M.; Neumann, R.; Ensinger, W.; Knoll, W.; Azzaroni, O. *Chem. Commun.* **2010**, *46*, 1908.
(28) Vlassiouk, I.; Siwy, Z. S. *Nano Lett.* **2007**, *7*, 552.
(29) Zhang, L. X.; Cai, S. L.; Zheng, Y. B.; Cao, X. H.; Li, Y. Q. *Adv. Funct. Mater.* **2011**, *21*, 2103.
(30) Kalman, E. B.; Vlassiouk, I.; Siwy, Z. S. *Adv. Mater.* **2008**, *20*, 293.
(31) Hou, X.; Yang, F.; Li, L.; Song, Y. L.; Jiang, L.; Zhu, D. B. *J. Am. Chem. Soc.* **2010**, *132*, 11736.
(32) Hou, X.; Liu, Y.; Dong, H.; Yang, F.; Li, L.; Jiang, L. *Adv. Mater.* **2010**, *22*, 2440.
(33) Apel, P. Y.; Blonskaya, I. V.; Orelovitch, O. L.; Dmitriev, S. N. *Nucl. Instrum. Methods Phys. Res., Sect. B* **2009**, *267*, 1023.
(34) Ali, M.; Yameen, B.; Cervera, J.; Ramirez, P.; Neumann, R.; Ensinger, W.; Knoll, W.; Azzaroni, O. *J. Am. Chem. Soc.* **2010**, *132*, 8338.
(35) Xie, Y.; Wang, X.; Xue, J.; Jin, K.; Chen, L.; Wang, Y. *Appl. Phys. Lett.* **2008**, *93*, 163116.
(36) Hou, X.; Zhang, H.; Jiang, L. *Angew. Chem., Int. Ed.* **2012**, *51*, 5296.
(37) Ali, M.; Ramirez, P.; Mafé, S.; Neumann, R.; Ensinger, W. *ACS Nano* **2009**, *3*, 603.
(38) Ali, M.; Mafe, S.; Ramirez, P.; Neumann, R.; Ensinger, W. *Langmuir* **2009**, *25*, 11993.
(39) Han, C. P.; Hou, X.; Zhang, H. C.; Guo, W.; Li, H. B.; Jiang, L. *J. Am. Chem. Soc.* **2011**, *133*, 7644.
(40) Ali, M.; Yameen, B.; Neumann, R.; Ensinger, W.; Knoll, W.; Azzaroni, O. *J. Am. Chem. Soc.* **2008**, *130*, 16351.
(41) Ali, M.; Schiedt, B.; Neumann, R.; Ensinger, W. *Macromol. Biosci.* **2010**, *10*, 28.
(42) Ali, M.; Neumann, R.; Ensinger, W. *ACS Nano* **2010**, *4*, 7267.
(43) Vlassiouk, I.; Kozel, T. R.; Siwy, Z. S. *J. Am. Chem. Soc.* **2009**, *131*, 8211.
(44) Tagliazucchi, M.; Azzaroni, O.; Szleifer, I. *J. Am. Chem. Soc.* **2010**, *132*, 12404.
(45) Tagliazucchi, M.; Rabin, Y.; Szleifer, I. *J. Am. Chem. Soc.* **2011**, *133*, 17753.
(46) Peleg, O.; Tagliazucchi, M.; Kröger, M.; Rabin, Y.; Szleifer, I. *ACS Nano* **2011**, *5*, 4737.
(47) Tagliazucchi, M.; Szleifer, I. *Soft Matter* **2012**, *8*, 7292.
(48) Apel, P. Y.; Blonskaya, I. V.; Didyk, A. Y.; Dmitriev, S. N.; Orelovitch, O. L.; Root, D.; Samoilova, L. I.; Vutsadakis, V. A. *Nucl. Instrum. Methods Phys. Res., Sect. B* **2001**, *179*, 55.
(49) Daiguji, H.; Oka, Y.; Shirono, K. *Nano Lett.* **2005**, *5*, 2274.
(50) Cervera, J.; Schiedt, B.; Neumann, R.; Mafe, S.; Ramirez, P. *J. Chem. Phys.* **2006**, *124*, 104706.
(51) Ramirez, P.; Apel, P. Y.; Cervera, J.; Mafe, S. *Nanotechnology* **2008**, *19*, 315707.
(52) Constantin, D.; Siwy, Z. S. *Phys. Rev. E* **2007**, *76*, 041202.
(53) Kosinska, I. D.; Goychuk, I.; Kostur, M.; Schmid, G.; Hanggi, P. *Phys. Rev. E* **2008**, *77*, 031131.
(54) Jardetzky, O. *Nature* **1966**, *27*, 969.
(55) Shigekawa, M.; Iwamoto, T. *Circ. Res.* **2001**, *88*, 864.
(56) Gadsby, D. C.; Takeuchi, A.; Artigas, P.; Reyes, N. *Philos. Trans. R. Soc., Lond. B* **2009**, *364*, 229.
(57) Moller, J. V.; Nissen, P.; Sorensen, T. L. M.; le Marie, M. *Curr. Opin. Struct. Biol.* **2005**, *15*, 387.
(58) Wen, L. P.; Hou, X.; Tian, Y.; Zhai, J.; Jiang, L. *Adv. Funct. Mater.* **2010**, *20*, 2636.